FULL PAPERS

Magnetic Resonance in Medicine 60:1011–1019 (2008)

Cellular-Interstitial Water Exchange and Its Effect on the Determination of Contrast Agent Concentration In Vivo: Dynamic Contrast-Enhanced MRI of Human Internal Obturator Muscle

David L. Buckley,[1]* Lucy E. Kershaw,[1] and Greg J. Stanisz[2]

The purpose of this study was to assess the effects of cellular-interstitial water exchange on estimates of tracer kinetics parameters obtained using rapid dynamic contrast-enhanced (DCE) MRI. Data from the internal obturator muscle of six patients were examined using three models of water exchange: no exchange (NX), fast exchange limit (FXL), and intermediate rate (shutter-speed [SS]). In combination with additional multiple flip angle (FA) data, a full two-pool exchange model was also used. The results obtained using the NX model (transfer constant, K^{trans} = 0.049 ± 0.027 min^{-1}, apparent interstitial volume, v_e = 0.14 ± 0.04) were marginally higher than those obtained using the FXL model (K^{trans} = 0.045 ± 0.025 min^{-1}, v_e = 0.13 ± 0.04), but the error bars overlapped in two-thirds of these parameter estimate pairs. Estimates of K^{trans} and v_e obtained using the SS model exceeded those obtained using the NX model in half the patients, and many estimates, including all those of intracellular residence time of water, t_i, were imprecise. Results obtained using the full two-pool model fell between those obtained using FXL and NX models, and estimates of t_i were also imprecise. The results suggest that data obtained using clinically relevant DCE-MRI are exchange-insensitive and unsuitable for the assessment of cellular-interstitial water exchange. Magn Reson Med 60:1011–1019, 2008. © 2008 Wiley-Liss, Inc.

Key words: transcytolemmal water exchange; dynamic contrast-enhanced MRI; tracer kinetics; T_1; quantitative MRI

It has been known for many years that the movement of water between tissue compartments can have a significant influence on measured tissue MR characteristics such as relaxation times and diffusion coefficients (e.g., Refs. 1 and 2). In recent years, there has been interest in how this exchange of water might affect tracer kinetics experiments performed using dynamic contrast-enhanced (DCE) MRI (3–6). In these studies it is usually assumed that water occupies four principal compartments: the intracellular space of the tissue, the interstitial space (extracellular extravascular space), the plasma space, and the red blood cells (RBC). It is broadly accepted that water exchange across the RBC membrane, between RBC and plasma, is extremely rapid due to the high water permeability of the membrane (mean residence time of water in the RBC = 9.8–14 ms [2]). That is, water exchange occurs at the so-called fast exchange limit (FXL). On the other hand, most evidence to date suggests that vascular-interstitial (also known as transendothelial) water exchange, between the blood plasma and interstitium, is relatively slow at less than 7 s^{-1} (3,4). There is little agreement about the rate of cellular-interstitial (also known as transcytolemmal) water exchange. Landis et al. (5) have suggested that this exchange may significantly influence the assessment of contrast agent concentrations in DCE-MRI experiments. Contrast agent enters the interstitium from the plasma and increases the relaxation rate of interstitial water. Since the relaxation rate of water in the cell remains the same, the increasing difference in compartmental rates may lead to significant transient sorties away from the precontrast water exchange state. Such an effect can result in underestimates in the measured tissue contrast agent concentration and subsequent inaccuracies in estimates of tracer kinetics parameters (5). Whether these effects are significant in a typical DCE-MRI experiment is the subject of debate (3,7,8).

In their previous work, Landis et al. (5) studied muscle. Muscle is of particular interest when assessing cellular-interstitial water exchange due to its structure. It has a large intracellular volume fraction, a much smaller interstitium, and a very small vascular fraction (9), and thus the MR signals obtained from muscle are largely insensitive to the confounding effects of vascular-interstitial water exchange. Following the lead of Landis et al. (5), we undertook a study of human muscle to address two principal aims. First, we assessed the maximum effect of cellular-interstitial water exchange on measurements of tracer kinetics parameters obtained using a clinically relevant DCE-MRI protocol by analyzing our data at the FXL and at the opposing limit of no exchange (NX) and comparing the results. Second, we used the approach described as the "shutter-speed" (SS) model (often referred to as bolus enhanced relaxation overview [BOLERO]) (5,6) to estimate the rate of cellular-interstitial water exchange in muscle. These findings led us to analyze our data further using a full two-pool exchange model.

[1]Imaging Science and Biomedical Engineering, University of Manchester, Manchester, UK.

[2]Department of Medical Biophysics, University of Toronto and Imaging Research, Sunnybrook Health Sciences Centre, Toronto, Canada.

Grant sponsors: Prostate Research Campaign UK; Terry Fox Programme, National Cancer Institute of Canada.

*Correspondence to: David L. Buckley, Ph.D., Imaging Science and Biomedical Engineering, University of Manchester, Stopford Building, Oxford Road, Manchester M13 9PT, UK. E-mail: david.buckley@manchester.ac.uk

Received 12 November 2007; revised 30 April 2008; accepted 11 June 2008.

DOI 10.1002/mrm.21748

Published online in Wiley InterScience (www.interscience.wiley.com).

THEORY

We assumed that muscle contains only two water compartments (intracellular and interstitial) (10) and used the subscripts *i* and *e* to refer to intracellular and interstitial water, respectively. These compartments have fractional pool sizes of p_i and p_e ($p_i + p_e = 1$) and inherent longitudinal relaxation rates of $R_{1(i)}$ ($= 1/T_{1(i)}$) and $R_{1(e)}$ ($= 1/T_{1(e)}$), respectively. Cellular-interstitial water exchange connects these compartments and the rate is described in terms of the mean residence time of water inside (t_i) and outside (t_e) the cells (the rate constants of water exchange are the inverse of the residence times); by conservation of mass, $t_e = p_e.t_i/p_i$. Longitudinal relaxation of the system was modified by the addition of a gadolinium-based contrast agent to the interstitial space. This system can be described using a two-pool exchange formalism (1). The solution has a biexponential form with the T_1 relaxation of the system described by two rate constants, R_{1S} and R_{1L}, and their respective fractional apparent populations, a_S and a_L, where $a_S + a_L = 1$ (10):

$$R_{1L} = \frac{1}{2}\left[R_{1(i)} + R_{1(e)} + r_1[Gd] + \frac{1}{t_i} + \frac{1}{t_e}\right] - \frac{1}{2}\left\{ \left[R_{1(i)} - R_{1(e)} - r_1[Gd] + \frac{1}{t_i} - \frac{1}{t_e}\right]^2 + \frac{4}{t_i t_e}\right\}^{1/2}, \quad [1]$$

$$R_{1S} = \frac{1}{2}\left[R_{1(i)} + R_{1(e)} + r_1[Gd] + \frac{1}{t_i} + \frac{1}{t_e}\right] + \frac{1}{2}\left\{ \left[R_{1(i)} - R_{1(e)} - r_1[Gd] + \frac{1}{t_i} - \frac{1}{t_e}\right]^2 + \frac{4}{t_i t_e}\right\}^{1/2}, \quad [2]$$

$$a_S = \frac{1}{2} - \frac{1}{2}\left(\frac{\left[(R_{1(i)} - R_{1(e)} - r_1[Gd]) \cdot (p_e - p_i) + \frac{1}{t_i} + \frac{1}{t_e}\right]}{\left\{ \left[R_{1(i)} - R_{1(e)} - r_1[Gd] + \frac{1}{t_i} - \frac{1}{t_e}\right]^2 + \frac{4}{t_i t_e}\right\}^{1/2}}\right), \quad [3]$$

where r_1 is the T_1 relaxivity of the contrast agent, and [Gd] is its concentration in the interstitial space. These equations contain three unknowns—[Gd], t_i, and p_e—since we assumed that $R_{1(e)} = R_{1(i)} = 1/T_{1(0)}$, where $T_{1(0)}$ is the longitudinal relaxation time of muscle measured prior to administration of contrast agent, and that $r_1 = 4.3\ mM^{-1}s^{-1}$ (11). Three different approximations were considered. In the FXL ($t_i \to 0$), the system (described using Eqs. [1]–[3]) is reduced to a single longitudinal relaxation rate, R_1:

$$R_1 = p_e(r_1[Gd] + R_{1(e)}) + p_i R_{1(i)}. \quad [4]$$

With NX ($t_i \to \infty$), Eqs. [1]–[3] are reduced to:

$$\begin{aligned} R_{1L} &= R_{1(i)} \\ R_{1S} &= R_{1(e)} + r_1[Gd] \\ a_S &= p_e \\ a_L &= p_i. \end{aligned} \quad [5]$$

In both approximations (FXL and NX) there are two unknowns: [Gd] and p_e. The third approximation to the full two-pool model was described by Landis et al. (5). The longitudinal relaxation of the system is described by a single exponential rate constant, R_{1L} ($\cong$ Eq. [1]):

$$R_1 = \frac{1}{2}\left[R_{1(i)} + R_{1(e)} + r_1[Gd] + \frac{1}{t_i} + \frac{1}{t_e}\right] - \frac{1}{2}\left\{ \left[R_{1(i)} - R_{1(e)} - r_1[Gd] + \frac{1}{t_i} - \frac{1}{t_e}\right]^2 + \frac{4}{t_i t_e}\right\}^{1/2}. \quad [6]$$

This empirical approximation has been called the SS model (6). Although in an algebraic sense the SS model differs from the full two-pool model, it contains the same three unknowns: [Gd], t_i, and p_e.

This left the task of estimating [Gd] as a function of time, and this was achieved through the use of DCE-MRI and tracer kinetics analysis (12). We modeled [Gd] as a convolution of the measured plasma arterial input function (AIF) with a conventional single-compartment model (13):

$$[Gd] = \frac{K^{trans}}{p_e}\int_0^t C_p(u)\exp\left(\frac{-K^{trans}}{p_e}(t-u)\right)du, \quad [7]$$

where K^{trans} is the volume transfer constant for contrast agent transport between the blood plasma and interstitium (12) and $C_p(t)$ is the plasma AIF. Thus by combining Eq. [7] with Eqs. [1]–[3], our solution to the full two-pool model had three unknowns: K^{trans}, p_e and t_i. The SS model was solved using a combination of Eq. [7] with Eq. [6] with the three unknowns, K^{trans}, p_e, and t_i. Equations [7] and [4] provided a solution to the FXL model, while Eqs. [7] and [5] combined to solve the NX model. Each of these solutions contained two unknowns: K^{trans} and p_e. It is conventional to report the fractional volumes, v_i and v_e, of the tissue compartments rather than the fractional pool sizes, p_i and p_e. The pool sizes match the volumes if the spin densities of the compartments are the same. In the absence of data to estimate the ratio of compartmental spin densities, we assume a ratio of 1 (thus $v_i = p_i$ and $v_e = p_e$) and report apparent volumes.

To compare the output of the model with the data acquired in our experiments, we needed to substitute the simulated relaxation rates of the four models into equations describing the signal obtained using our imaging sequence (14). In the case of the FXL and SS models, the resultant single-component R_1 was substituted directly into:

$$S = S_0\frac{\sin(\alpha)[1 - \exp(-TR.R_1)]}{[1 - \cos(\alpha)\exp(-TR.R_1)]}, \quad [8]$$

where S_0 is the signal that would be obtained from the tissue using an infinite repetition time (TR) and a 90° pulse, and α is the actual flip angle (FA) used. The S_0 term incorporates the effects of T_2^* decay (which is assumed to vary negligibly at short echo times [TEs]), scaling factors, and other sequence settings that may confound signal-intensity comparisons. The NX and full two-pool models

have biexponential solutions and the R_{1S} and R_{1L} components are substituted into:

$$S = S_0\left\{ a_S\frac{\sin(\alpha)[1-\exp(-TR.R_{1S})]}{[1-\cos(\alpha)\exp(-TR.R_{1S})]} + a_L\frac{\sin(\alpha)[1-\exp(-TR.R_{1L})]}{[1-\cos(\alpha)\exp(-TR.R_{1L})]}\right\}. \quad [9]$$

MATERIALS AND METHODS

Six patients (age = 60–77 years, mean = 68 years) were examined; all were undergoing MRI for assessment of benign prostatic hyperplasia (15). The study was performed at 1.5 T (Philips Intera; Philips Medical Systems, Best, The Netherlands) using a cardiac phased-array coil wrapped around the pelvis for signal detection. Following the acquisition of scout images and reference images for coil scaling and parallel reconstruction (SENSE reference), the pelvis was imaged in the axial plane using a multislice turbo spin-echo sequence (20 slices; 512 × 512 matrix; 400 × 400 mm FOV; 4.5 mm slice thickness; 0.5 mm gap; TR/TE(effective) = 5432/135 ms; echo train length = 19; four averages). A 400 × 400 × 100 mm volume aligned in the axial plane and including the prostate, internal obturator muscles, and bladder was then selected for all subsequent quantitative imaging. The $T_{1(0)}$ of tissues in this volume was measured using a multishot 3D inversion recovery turbo field echo (IR-TFE) sequence and inversion times of 65, 250, 1000, 2500, and 3900 ms (176 × 176 × 20 matrix (following interpolation); TR/TE = 2.4/0.8 ms; intershot delay = 4 s; SENSE factor of 2.5 applied left to right). Subsequently, a 3D fast field echo (RF-spoiled gradient echo) sequence was used to acquire 10 volumes at each of the following FAs, 30°, 5°, and 50°, to establish baseline signal intensities (176 × 112 × 10 acquisition matrix (176 × 176 × 20 following interpolation); TR/TE = 3.4/0.9 ms; SENSE factor of 2.5). The 30° acquisition was then repeated every 1.5 s for 7.5 min following injection of 0.1 mmol/kg Gd-DTPA-BMA (Omniscan; GE Healthcare, Little Chalfont, Buckinghamshire, UK). The contrast agent was injected at 3 ml/s using a power injector (Spectris; Medrad, Indianola, PA, USA) and was followed by a similar volume of saline. At the end of the dynamic run, a further 10 volumes were again acquired at FAs of 30°, 5°, and 50°.

The plasma AIF was obtained by examining data measured in the external iliac arteries in the inferior half of the imaging volume. The distal aspect of the arteries within the volume was selected to avoid in-flow artifacts (16). Signal intensity-time curves were plotted for all voxels in 5 × 5 grids placed over each artery. These were converted to R_1-time curves by reference to the baseline signal intensity (before the first pass of contrast agent) (17), the measured hematocrit of the blood, and by assuming a baseline blood T_1 of 1400 ms (18,19). Voxels exhibiting partial volume effects were rejected (that is, if they showed a reduced first-pass peak height compared to those in the center of the artery). The R_1-time curves from the remaining voxels were averaged together, and the mean time course from the left and right arteries was used as an AIF. A volume of muscle tissue (internal obturator) was selected for further analysis. $S_0(30)$, $S_0(5)$, and $S_0(50)$ for the muscle were calculated for each FA data set (5°, 30°, and 50°) using baseline data and the $T_{1(0)}$ estimate derived from IR-TFE data (20). Postcontrast data were divided by the respective S_0 estimates to provide raw signal intensity-time curves for the dynamic data and 5°, 30°, and 50° data in the tail of the muscle signal-time curve for subsequent model fitting.

Fitting was performed using the sequential quadratic programming algorithm (21) of the MATLAB software package (The MathWorks Inc., Natick, MA, USA). The minimization function, reduced chi-squared (χ_0^2 was defined as:

$$\chi_0^2 = \frac{1}{N-n-1}\sum_{i=1}^{N}\frac{(fit_i - data_i)^2}{\sigma_i^2}, \quad [10]$$

where N is the number of data points, n is the number of fitted parameters, σ_i is the standard error of each measured point (assumed to be independent of [Gd]) estimated from the standard deviation of the first 10 dynamic data points, before contrast agent injection. The FXL, NX and SS models were each fitted to the raw dynamic signal-time curves using the measured AIFs and baseline $T_{1(0)}$ estimates. This produced three estimates of K^{trans}: K^{trans}(FXL), K^{trans}(NX), and K^{trans}(SS); three estimates of v_e: v_e(FXL), v_e(NX), and v_e(SS); and one estimate of t_i: t_i(SS). The precision of these estimates was assessed using a bootstrap technique (9).

To address concerns raised following the above comparisons (see Discussion), the full two-pool exchange model was fitted simultaneously to all the postcontrast data (30° dynamic and 5°, 50° and 30° post-dynamic data). This provided estimates of K^{trans}(full), v_e(full), and t_i(full). The precision of the fitted parameters and parameter coupling was defined in terms of confidence regions (22). The confidence region of a fitted parameter was determined by finding the maximum and minimum values of the parameter while optimizing all remaining parameters such that:

$$\chi^2 = \chi_0^2\left(1 + \frac{n}{N-n}F(n,N-n,p)\right), \quad [11]$$

where p is the desired confidence level (95%) and F is the F distribution function (22). This procedure determined not only the precision of fitted parameters, but also coupling between them.

RESULTS

The subjects studied had measured hematocrit levels ranging from 0.37 to 0.45 (mean = 0.42) and DCE-MRI data were acquired successfully from all six subjects. An AIF was extracted from each subject using an average of 7 ± 3 voxels and the baseline $T_{1(0)}$ of muscle (median volume assessed = 12 ml, range = 4–68 ml) was estimated to be 1060 ± 30 ms. An example image and signal-time data from the external iliacs of subject 1 are shown in Fig. 1. Both the FXL and NX models produced acceptable fits to the data (mean $\chi_0^2 < 1.4$), with the average χ_0^2 obtained with the NX model being marginally smaller than that obtained

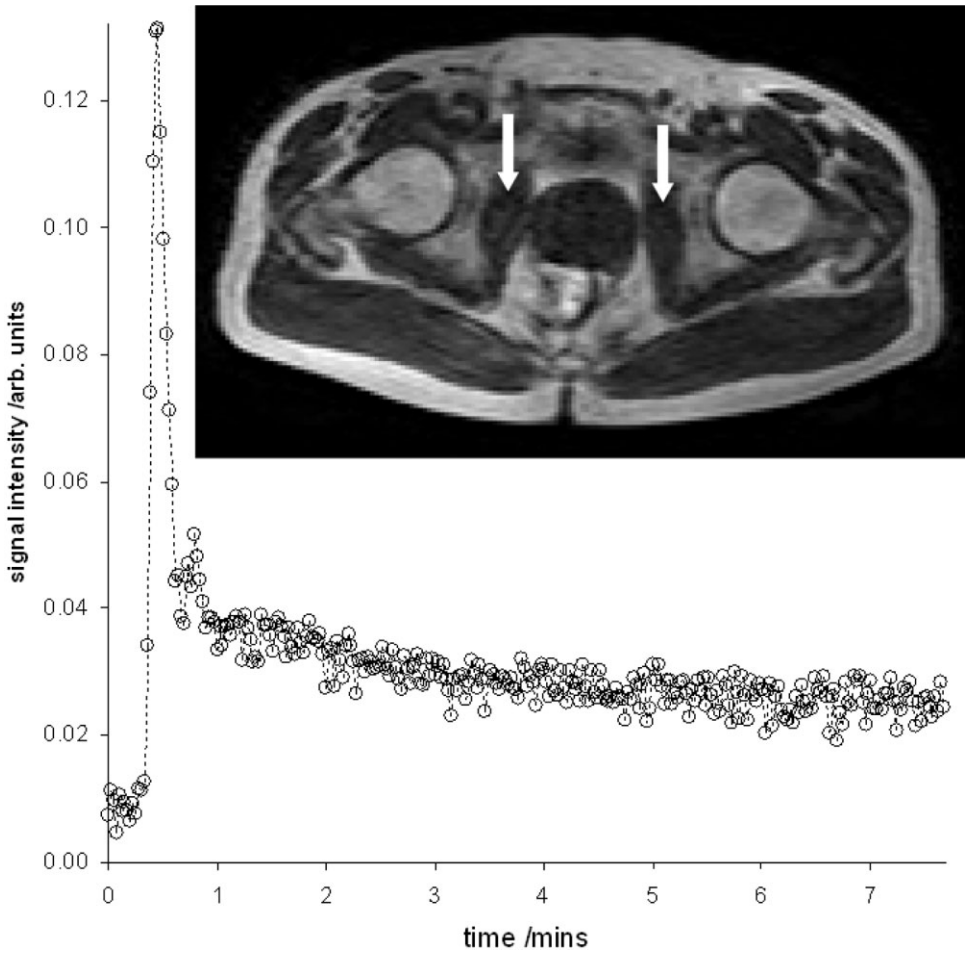

FIG. 1. Signal-time data measured in the external iliac arteries of subject 1. A single section from the center of the imaging volume acquired in the same subject is overlaid with the internal obturator muscles highlighted with arrows. This image, acquired using a RF-spoiled gradient-echo sequence, was obtained prior to arrival of the contrast agent and contains no evidence of in-flow artifact in the vessels.

using the FXL model (Table 1). Estimates of K^{trans}(NX) were on average 7% higher than estimates of K^{trans}(FXL). Estimates of v_e(NX) were on average 9% higher than estimates of v_e(FXL) (see Tables 2 and 3). Fits obtained using the SS model resulted in decreased χ_0^2 compared to the FXL and NX model fits in three of six cases (Table 1), but none of these decreases were statistically significant when set against the decrease in degrees of freedom of the model (assessed using an F-test).

Table 1
Reduced χ_0^2 Resulting From the Fits of the Four Water Exchange Models to the Data Obtained in All Six Subjects

	χ_0^2(FXL)	χ_0^2(NX)	χ_0^2(SS)	χ_0^2(full)[a]
Subject 1	1.04	1.01	0.96	1.05
Subject 2	0.74	0.74	0.74	0.99
Subject 3	1.84	1.81	1.69	1.69
Subject 4	1.81	1.80	1.80	1.50
Subject 5	1.84	1.79	1.65	1.76
Subject 6	1.11	1.11	1.11	0.99
Mean (SD)	1.39 (0.5)	1.38 (0.5)	1.33 (0.4)	1.33 (0.4)

[a]Note that χ_0^2 (full) is calculated using dynamic and postdynamic data while the other χ_0^2 values are calculated using the dynamic data only.

Estimates of parameter precision and coupling confirmed that the two-pool model was sufficient to describe the experimental data. A preliminary assessment using a four-pool model (RBC, plasma, and intracellular and interstitial spaces) resulted in significant parameter coupling, and those parameters associated with RBC-plasma exchange and vascular-interstitial exchange could not be determined. Fits to the two-pool model compared well with those obtained using the SS model (see Figs. 2 and 3). Conversely, the estimates of K^{trans}(full) and v_e(full) were closer to those obtained using the FXL and NX models than those obtained using the SS model (Tables 2 and 3). Estimates of t_i(full) ranged from 0.5 to 4.2 s; most were very imprecise (Table 4) and were different from the estimates of t_i(SS) (which ranged from 0 to 1.6 s).

DISCUSSION

Despite a succession of studies over the years, there remains considerable uncertainty surrounding the rate of cellular-interstitial water exchange (3–5,23). Sobol et al.

Table 2
Estimates of the Volume Transfer Constant, K^{trans}, and Its Precision Obtained in Six Subjects Using the Four Water Exchange Models

	K^{trans}(FXL) (10^{-3} min^{-1})	K^{trans}(NX) (10^{-3} min^{-1})	K^{trans}(SS) (10^{-3} min^{-1})	K^{trans}(full) (10^{-3} min^{-1})
Subject 1	60 ± 1	66 ± 1	93 ± 9[a]	60 ± 4
Subject 2	15.7 ± 0.2	16.4 ± 0.3	15.7 ± 0.6	16.7 ± 1.0
Subject 3	29 ± 1	31 ± 1	44 ± 4[a]	29 ± 3
Subject 4	24 ± 1	26 ± 1	31 ± 6	26 ± 4
Subject 5	75 ± 2	82 ± 2	147 ± 20[a]	76 ± 7
Subject 6	68 ± 3	71 ± 4	68 ± 10	75 ± 10
Mean (SD)	45 (25)	49 (27)	67 (48)	47 (26)

[a]Estimates obtained using the SS model that were significantly higher than those obtained with the other models.

(23) arrived at estimates in muscle in vitro suggesting an exchange rate of 50 s^{-1}. Donahue et al. (3) estimated rates in a perfused heart model of between 8 and 27 s^{-1}. More recently, Landis et al. (5) suggested that exchange rates for rat skeletal muscle in vivo fall at the lower end of Donahue et al.'s predictions. Our data in human internal obturator muscle in vivo appear to support the findings of Landis et al. (5) but highlight the imprecision of such measurements made using DCE-MRI data alone. The cellular-interstitial exchange rate (defined as $1/t_i + 1/t_e$) estimated using the two-pool model in our six subjects ranged from 1.4 to 16.6 s^{-1}.

The primary finding of this study may be of particular interest to those involved in DCE-MRI in the laboratory or clinic. When typical rapid spoiled gradient-echo sequences and a standard dose of contrast agent are employed, the influence of cellular-interstitial water exchange on the determination of contrast agent concentration in muscle is small. This is appreciated most clearly in the comparison of FXL and NX analyses (Tables 2 and 3). Despite the relatively high precision of these measurements, the 95% confidence intervals of the paired estimates of K^{trans}(FXL) and K^{trans}(NX) and the paired estimates of v_e(FXL) and v_e(NX) overlap in two-thirds of the cases. It is important to emphasize that the FXL and NX models represent the limits of the effect of cellular-interstitial water exchange on our DCE-MRI experiment; our findings suggest that the combination of a 30° FA, a short TR (3.4 ms), and a standard 0.1 mmol/kg dose of contrast agent appears to have been sufficient to achieve exchange minimization (24).

Analysis of the same data using the SS technique produced contradictory results. Despite the fact that this technique purports to allow for intermediate exchange rates, the estimates of both K^{trans}(SS) and v_e(SS) lay above the upper limit determined by the NX results in half the cases. Furthermore, the error bars on the estimates of v_e(SS) and t_i(SS) were often excessively large. Examination of the distribution of bootstrap estimates suggests that there are strong correlations between estimates of v_e(SS) and t_i(SS) in half the cases (Fig. 4a) and strong correlations between v_e(SS) and K^{trans}(SS) in two others (Fig. 4b). The t_i(SS) estimate obtained in the remaining case (subject 6) was 0 s; the SS model had collapsed to a limiting case equivalent to the FXL model. In two cases the bootstrap distributions contained two distinct minima with physiologically plausible solutions (large v_e and long t_i or small v_e and short t_i). These results contrast starkly with the distribution of bootstrap estimates obtained using the FXL and NX models (Fig. 5). Taken together, these results raise questions about the validity of the SS approach when applied to DCE-MRI data acquired in a way similar to our own (e.g., Refs. 25–27). Essentially, the SS model is over parameterized—two parameters (K^{trans} and v_e) are sufficient to describe the data; the use of three parameters results in coupling and the estimates are compromised. The likely reason for the bias obtained with the SS model in half our cases has been discussed in the past (7,8) and subsequently addressed by Yankeelov et al. (6) using an extended version of the SS model similar to the full two-pool model. If we plot calibration curves of [Gd] against a simulated signal intensity obtained using the imaging sequence employed here and the average muscle parameters estimated using the two-pool model (Tables 2–4), we see a pattern closely matching the signal resulting from the NX model (Fig. 6). Both curves are almost indistinguishable from the FXL signal up to contrast agent concentrations of ~0.5 mM, and all remain very close up to the maximum interstitial concen-

Table 3
Estimates of the Apparent Interstitial Volume Fraction, v_e, and Its Precision Obtained in Six Subjects Using the Four Water Exchange Models

	v_e(FXL)	v_e(NX)	v_e(SS)	v_e(full)
Subject 1	0.11 ± 0.001	0.12 ± 0.001	0.17 ± 0.02[a]	0.12 ± 0.006
Subject 2	0.11 ± 0.003	0.13 ± 0.004	0.11 ± 0.34	0.13 ± 0.006
Subject 3	0.12 ± 0.003	0.13 ± 0.003	0.46 ± 0.2[a]	0.13 ± 0.007
Subject 4	0.08 ± 0.003	0.09 ± 0.003	0.12 ± 0.4	0.10 ± 0.01
Subject 5	0.18 ± 0.002	0.20 ± 0.003	0.35 ± 0.05[a]	0.19 ± 0.01
Subject 6	0.16 ± 0.004	0.17 ± 0.004	0.16 ± 0.03	0.19 ± 0.02
Mean (SD)	0.13 (0.04)	0.14 (0.04)	0.23 (0.14)	0.14 (0.04)

[a]Estimates obtained using the SS model that were significantly higher than those obtained with the other models.

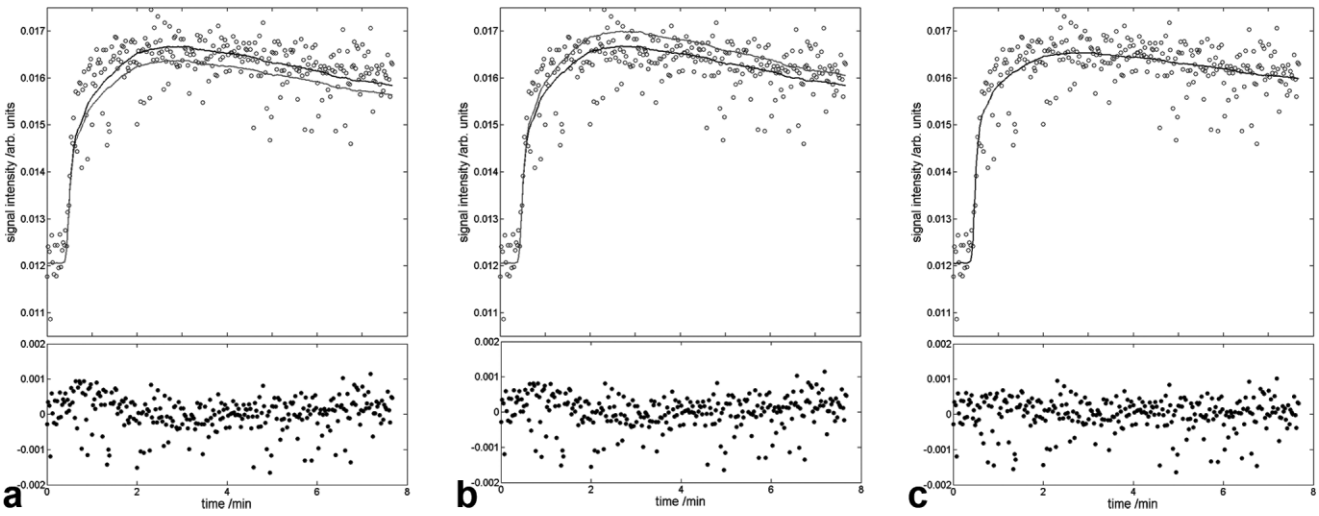

FIG. 2. Fits of the water exchange models (black lines) to signal-time data from subject 1 using the (**a**) FXL model, (**b**) NX model, and (**c**) SS model. Residuals are plotted below each curve. To highlight the subtle effect of exchange on these data, additional curves were simulated using the best fit parameters obtained using the FXL and NX models but with the assumptions of the NX and FXL, respectively. These can be seen as gray lines in a and b lying below and above the fitted curves, respectively.

tration attained in this study, which was typically < 1.0 mM. This can be contrasted with the calibration curve obtained using the SS model; the concentration of contrast agent inferred from such a curve would be significantly overestimated. This divergent behavior results directly from the assumption in the SS model that the relaxation rate of the tissue can be approximated using only the long component, R_{1L}, of the two-pool exchange solution (5). The longitudinal signal recovery (T_1 relaxation) can be described by a single exponential *only* when water exchange is in the FXL and total mixing of the pools is observed. In all other scenarios there is no single rate constant to describe the recovery, and a biexponential solution is necessary to describe the observed signal. The increasing contribution of the second component, R_{1S}, can be seen in the lower half of Fig. 6 despite the assertion that this component is "rendered miniscule by the exchange kinetics" (5). In the example shown in Fig. 6 (and in at least half of the patient data in this study) the SS model assumptions are incorrect and the model is inappropriate for such analyses. The FXL and NX models are better choices for an assessment of tracer kinetics parameters, while the full two-pool treatment is essential for an accurate (if not precise) assessment of cellular-interstitial water exchange.

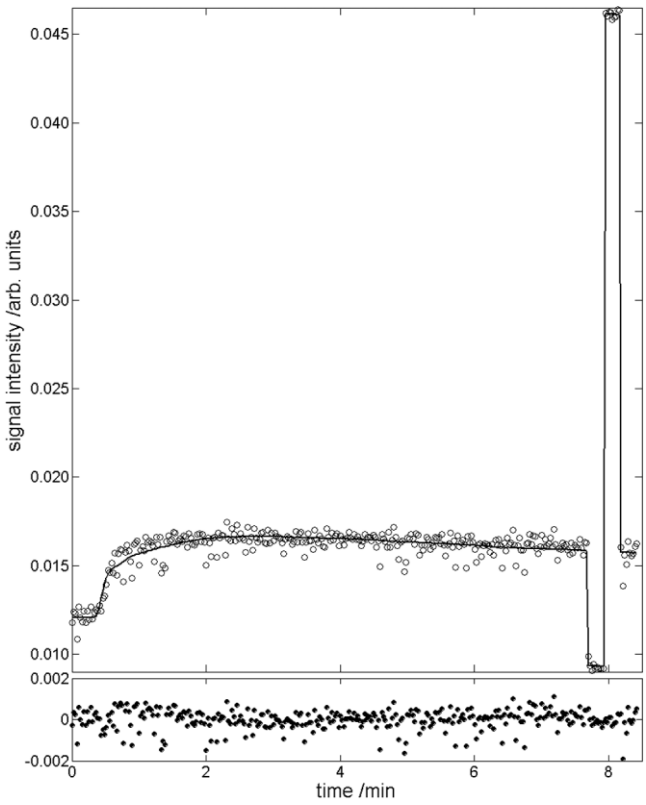

FIG. 3. Fit of the full two-pool water exchange model to signal-time data from subject 1 including post-dynamic data acquired at 50°, 5°, and 30°, respectively. Note the large changes in signal resulting from the changes in FA employed. Residuals are plotted below the curve.

This leaves the question of whether our data are sufficient for an assessment of the water exchange rate. The 30° dynamic data alone were shown to be exchange-mini-

Table 4
Estimates of the Cellular Residence Time, t_i, and Its Precision Obtained in Six Subjects Using Two of the Water Exchange Models

	t_i(SS) (s)	t_i(full) (s)
Subject 1	1.1 ± 0.2	0.5 ± 0.5
Subject 2	0.003 ± 0.8	2.2 ± 0.8
Subject 3	1.6 ± 0.3	4.2 ± 3.3
Subject 4	0.8 ± 0.8	2.8 ± 2.0
Subject 5	0.7 ± 0.1	3.8 ± 23
Subject 6	0.0 ± 0.3	2.3 ± 4.8
Mean (SD)	0.69 (0.61)	2.6 (1.3)

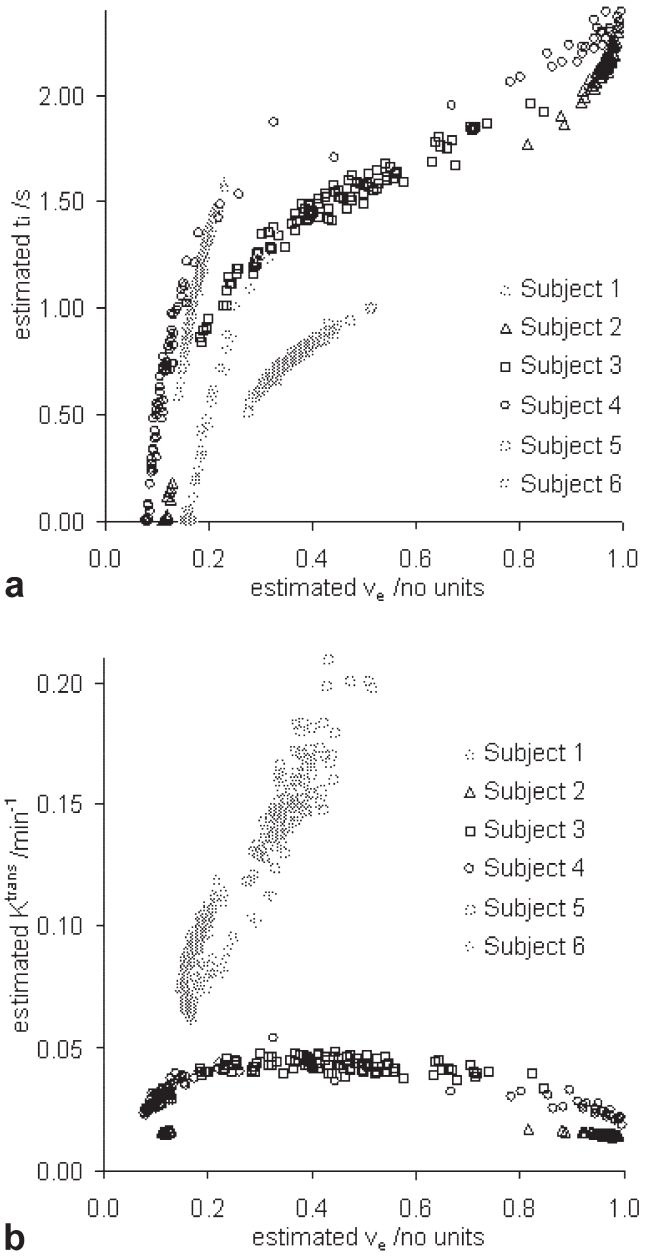

FIG. 4. Bootstrap estimates of v_e(SS) against t_i(SS) (**a**) and v_e(SS) against K^{trans}(SS) (**b**). Note the poor precision (large scatter) in t_i(SS) for all subjects. There is poor precision in v_e(SS) for three subjects (black symbols), and in two of the remaining subjects (1 and 5) there is poor precision in estimates of K^{trans}(SS) (b).

mized and therefore unsuitable for such an assessment (24). The inclusion of 5° and 50° data was designed to extend the range of exchange sensitivity of the acquisition. That is, the 5° data were more sensitive and the 50° data less sensitive than the 30° data. The full two-pool model was able to predict the amplitude of the 5° and 50° data with negligible systematic error (Fig. 3). We were able to obtain estimates of t_i(full) while maintaining estimates of K^{trans}(full) and v_e(full) within the bounds dictated by the FXL and NX models. However, the estimates of t_i(full) were imprecise and showed a high intersubject variability. Future studies that aim to measure water exchange will require significantly more exchange sensitive data (e.g., by including steady-state data with contrast agent titration [28]).

Study Limitations

We assumed, in the absence of data to confirm otherwise, that the underlying spin densities and T_1 relaxation rates of the interstitial and intracellular spaces were the same, that the relaxivity of Gd-DTPA-BMA in the interstitium was the same as that in the blood plasma, and that the

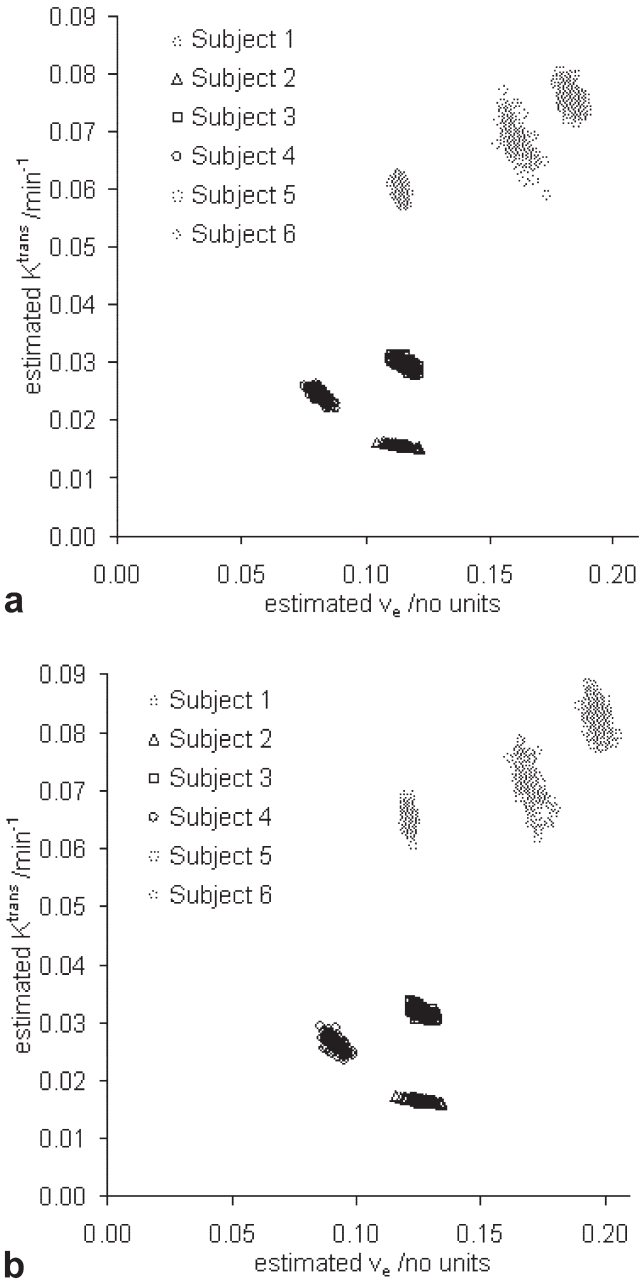

FIG. 5. Bootstrap estimates of v_e(FXL) against K^{trans}(FXL) (**a**) and v_e(NX) against K^{trans}(NX) (**b**). Note the relatively high precision of both parameters for all subjects and both models, emphasized further by the smaller scale used for the axes compared with Fig. 4b.

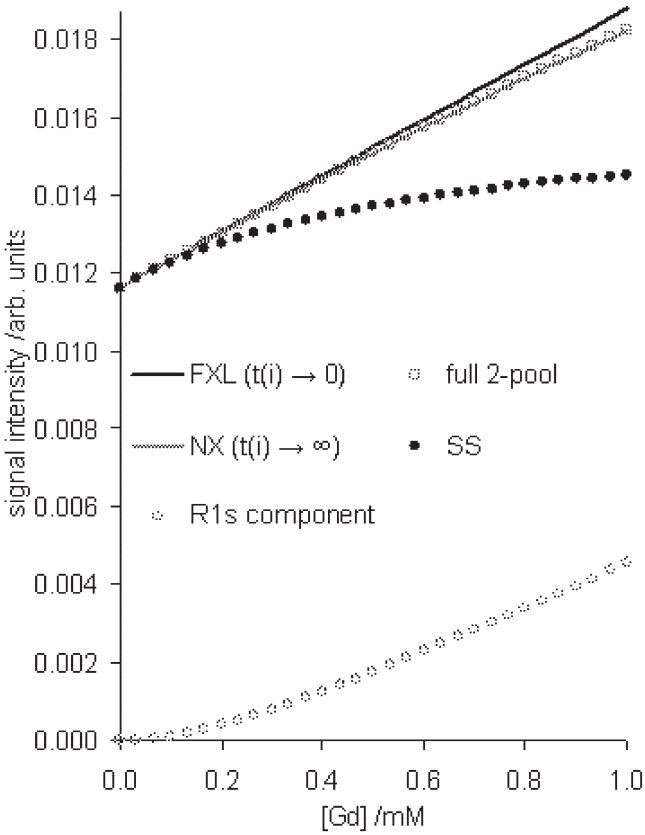

FIG. 6. Calibration curves relating measured signal intensity to interstitial contrast agent concentration for average muscle parameters $T_{1(0)}$ = 1060 ms, t_i = 2.6 s, and v_e = 0.14) and the imaging sequence employed in this study (TR = 3.4 ms, FA = 30°). Other details are described in the text. A separate curve is calculated for each water exchange model; the NX and full two-pool curves effectively overlap. The signal contribution from the R_{1S} component of the full two-pool model (ignored in the SS model) is also shown.

Gd-DTPA-BMA did not enter the cells. These assumptions, if in error (e.g., Ref. 29), will introduce bias into our parameter estimates, but are unlikely to change the general conclusions of the study.

These data were acquired as part of a study designed to measure prostate blood flow that required a high temporal resolution (9,15), and as such, the signal-to-noise ratio (SNR) was limited. As proposed by Landis et al. (5), the signal from intravascular water was assumed to be negligible, and a preliminary analysis using a four-pool model (compare with Ref. 30) indicated that there was insufficient information in these data to support its inclusion. We can therefore infer that its exclusion introduced little bias into our analysis. However, it is known from similar studies that the intravascular water signal can be measured using a distributed parameter model and an FXL approximation, and that this pool represents around 3% of the tissue water volume (9). For example, in one of the six subjects studied, there is evidence for some bias in the FXL and NX fits (Fig. 2a and b, temporal structure in the residuals) that is removed following a distributed parameter/FXL fit (not shown). A similar improvement in fit quality is obtained following the SS model fit (Fig. 2c), an effect that has been reported before (6,27). Despite this, the full two-pool model fit (Fig. 3) does not remove the bias (the residuals match those of the NX fit). Not for the first time in this study, the SS model approximation did not reflect the predictions of its parent model.

CONCLUSIONS

Using a clinically relevant DCE-MRI acquisition, data were obtained from the internal obturator muscle in an exchange-minimized manner with little or no influence from cellular-interstitial water exchange. Analysis of such data using an SS approach should be approached with caution as estimates of K^{trans} and v_e may be biased, estimates of t_i may be inaccurate, and many parameter estimates are likely to be imprecise. Though it was possible to estimate t_i using data with a range of FAs and a two-pool model, these estimates were very imprecise and our findings suggest that DCE-MRI data of this type, when used in isolation, are unsuitable for the assessment of water exchange.

ACKNOWLEDGMENT

Lucy Kershaw was supported by an MRC studentship.

REFERENCES

1. Hazlewood CF, Chang DC, Nichols BL, Woessner DE. Nuclear magnetic resonance transverse relaxation times of water protons in skeletal muscle. Biophys J 1974;14:583–606.
2. Herbst MD, Goldstein JH. A review of water diffusion measurement by NMR in human red blood cells. Am J Physiol 1989;256:C1097–C1104.
3. Donahue KM, Burstein D, Manning WJ, Gray ML. Studies of Gd-DTPA relaxivity and proton-exchange rates in tissue. Magn Reson Med 1994; 32:66–76.
4. Judd RM, Reeder SB, May-Newman K. Effects of water exchange on the measurement of myocardial perfusion using paramagnetic contrast agents. Magn Reson Med 1999;41:334–342.
5. Landis CS, Li X, Telang FW, Coderre JA, Micca PL, Rooney WD, Latour LL, Vetek G, Palyka I, Springer CS. Determination of the MRI contrast agent concentration time course in vivo following bolus injection: effect of equilibrium transcytolemmal water exchange. Magn Reson Med 2000;44:563–574.
6. Yankeelov TE, Rooney WD, Li X, Springer CS. Variation of the relaxographic "shutter-speed" for transcytolemmal water exchange affects the CR bolus-tracking curve shape. Magn Reson Med 2003;50:1151–1169.
7. Buckley DL. Transcytolemmal water exchange and its affect on the determination of contrast agent concentration in vivo. Magn Reson Med 2002;47:420–421.
8. Springer CS, Rooney WD, Li X. The effects of equilibrium transcytolemmal water exchange on the determination of contrast reagent concentration in vivo. Magn Reson Med 2002;47:422–424.
9. Kershaw LE, Buckley DL. Precision in measurements of perfusion and microvascular permeability with T1-weighted dynamic contrast-enhanced MRI. Magn Reson Med 2006;56:986–992.
10. Landis CS, Li X, Telang FW, Molina PE, Palyka I, Vetek G, Springer CS. Equilibrium transcytolemmal water-exchange kinetics in skeletal muscle in vivo. Magn Reson Med 1999;42:467–478.
11. Morkenborg J, Taagehoj JF, Vaever PN, Frokiaer J, Djurhuus JC, Stodkilde-Jorgensen H. In vivo measurement of T1 and T2 relaxivity in the kidney cortex of the pig—based on a two-compartment steady-state model. Magn Reson Imaging 1998;16:933–942.
12. Tofts PS, Brix G, Buckley DL, Evelhoch JL, Henderson E, Knopp MV, Larsson HB, Lee TY, Mayr NA, Parker GJ, Port RE, Taylor J, Weisskoff RM. Estimating kinetic parameters from dynamic contrast-enhanced T1-weighted MRI of a diffusable tracer: standardized quantities and symbols. J Magn Reson Imaging 1999;10:223–232.

13. Tofts PS. Modeling tracer kinetics in dynamic Gd-DTPA MR imaging. J Magn Reson Imaging 1997;7:91–101.
14. Haase A, Frahm J, Matthaei D, Hanicke W, Merboldt KD. FLASH imaging—rapid NMR imaging using low flip-angle pulses. J Magn Reson 1986;67:258–266.
15. Kershaw LE, Hutchinson CE, Allen PD, Buckley DL. Functional imaging of the prostate: quantitative DCE-MRI and its repeatability. In: Proceedings of the 15th Annual Meeting of ISMRM, Berlin, Germany, 2007 (Abstract 795).
16. Parker GJ, Roberts C, Macdonald A, Buonaccorsi GA, Cheung S, Buckley DL, Jackson A, Watson Y, Davies K, Jayson GC. Experimentally-derived functional form for a population-averaged high-temporal-resolution arterial input function for dynamic contrast-enhanced MRI. Magn Reson Med 2006;56:993–1000.
17. Buckley DL, Roberts C, Parker GJ, Logue JP, Hutchinson CE. Prostate cancer: evaluation of vascular characteristics with dynamic contrast-enhanced T1-weighted MR imaging—initial experience. Radiology 2004;233:709–715.
18. Flacke SJ, Fischer SE, Lorenz CH. Measurement of the gadopentetate dimeglumine partition coefficient in human myocardium in vivo: normal distribution and elevation in acute and chronic infarction. Radiology 2001;218:703–710.
19. Lu H, Golay X, Pekar JJ, Van Zijl PC. Functional magnetic resonance imaging based on changes in vascular space occupancy. Magn Reson Med 2003;50:263–274.
20. Larsson HBW, Rosenbaum S, Fritz-Hansen T. Quantification of the effect of water exchange in dynamic contrast MRI perfusion measurements in the brain and heart. Magn Reson Med 2001;46:272–281.
21. Powell MJD. Numerical analysis. New York: Springer Verlag; 1978.
22. Draper NR, Smith H, editors. Applied regression analysis. New York: John Wiley and Sons; 1981.
23. Sobol WT, Jackels SC, Cothran RL, Hinson WH. NMR spin-lattice relaxation in tissues with high concentration of paramagnetic contrast media: evaluation of water exchange rates in intact rat muscle. Med Phys 1991;18:243–250.
24. Donahue KM, Weisskoff RM, Chesler DA, Kwong KK, Bogdanov Jr AA, Mandeville JB, Rosen BR. Improving MR quantification of regional blood volume with intravascular T1 contrast agents: accuracy, precision, and water exchange. Magn Reson Med 1996;36:858–867.
25. Yankeelov TE, Rooney WD, Huang W, Dyke JP, Li X, Tudorica A, Lee JH, Koutcher JA, Springer CS. Evidence for shutter-speed variation in CR bolus-tracking studies of human pathology. NMR Biomed 2005;18:173–185.
26. Li X, Huang W, Yankeelov TE, Tudorica A, Rooney WD, Springer Jr CS. Shutter-speed analysis of contrast reagent bolus-tracking data: preliminary observations in benign and malignant breast disease. Magn Reson Med 2005;53:724–729.
27. Kim S, Quon H, Loevner LA, Rosen MA, Dougherty L, Kilger AM, Glickson JD, Poptani H. Transcytolemmal water exchange in pharmacokinetic analysis of dynamic contrast-enhanced MRI data in squamous cell carcinoma of the head and neck. J Magn Reson Imaging 2007;26:1607–1617.
28. Wacker CM, Wiesmann F, Bock M, Jakob P, Sandstede JJW, Lehning A, Ertl G, Schad LR, Haase A, Bauer WR. Determination of regional blood volume and intra-extracapillary water exchange in human myocardium using feruglose: first clinical results in patients with coronary artery disease. Magn Reson Med 2002;47:1013–1016.
29. Stanisz GJ, Henkelman RM. Gd-DTPA relaxivity depends on macromolecular content. Magn Reson Med 2000;44:665–667.
30. Li X, Rooney WD, Springer Jr CS. A unified magnetic resonance imaging pharmacokinetic theory: intravascular and extracellular contrast reagents. Magn Reson Med 2005;54:1351–1359.